CHAPTER 4

Dielectric, elastic and viscous properties of some binary mixtures of hockey stick-shaped mesogen and octyloxy-cyano-biphenyl

4.1. Introduction

Investigation of different physical properties of liquid crystal (LC) mesophases is quite interesting from the application point of view in display as well as non-display photonic and electro-optic devices such as laser beam steering [1], phase modulator [2], optical shutter [3-5] etc. The advantageous feature of the nematic phase is to produce a mechanical distortion of the molecules in response to an external field, resulting in an electric polarization within the system [6]. The nematic liquid crystal compounds with desirable physical properties like high optical birefringence (Δn), high dielectric anisotropy ($\Delta\varepsilon$), wide nematic phase range, low rotational viscosity (γ_1), good thermal and photostability, greater response to the external field etc. are most efficient in many practical applications [7]. A highly conjugated liquid crystal compound with high optical birefringence also exhibits a high rotational viscosity due to the effect of moment of inertia. However, the most promising criterion to upgrade the nematic liquid crystal is to enhance its optical birefringence along with the reduction of the rotational viscosity [8,9]. Performance of the electro-optical devices is based on the molecular switching behavior which is associated with the relaxation or response time τ_0. Till date several physical properties have been studied in pure nematic liquid crystal compounds having different molecular geometry such as rod-like, bent-core, hockey-stick shaped, disc-like etc. Different calamitic compounds has been found to exhibit high positive dielectric anisotropy [10,11], wide nematic mesophase stability [12] and low rotational viscosity etc. In addition to the principle director $\hat{n}$ like the calamitic molecules, the bent-core (BC) molecules are found to exhibit a much faster switching behavior of the secondary director $\hat{m}$, perpendicular to $\hat{n}$ [13,14]. Moreover, the BC nematogens have smectic-like small cybotactic clusters which further affects the physical properties of the system [15,16]. Due to the existence of such unusual characteristics in BC systems in their nematic phase, they reveal stable uniaxial and biaxial nematic

phases [17-20], different unusual smectic mesophases [21,22], giant flexo-electric response [23], dielectric anisotropy with a crossover nature [24,25] and atypical negative values of bend-splay anisotropy [26-28]. Moreover, the BC compounds also have large relaxation time (τ_0) and thereby greater value of the rotational viscosity (γ_1) [29-31] which resists them in fast switching electro-optical devices. On the other hand, the hockey stick-shaped molecules possess a shape intermediate between the calamitic and conventional bent-core molecules exhibiting a lower value of γ_1 relative to the symmetric bent-core molecules [25]. A number of efforts have been devoted to develop the physical properties of nematic LC compound and make an enormous use in display and non-display technological applications as per requirement [17,18,32-34]. However, any single mesogenic compound cannot fulfill all the desired properties for the multipurpose application. Therefore, the interest has grown to mix several components of liquid crystal compounds at a particular proportion and achieve the desired property. The mixture of LC compounds having divergent molecular structure has been found to critically optimize the properties of individual constituents.

In this chapter, the static dielectric permittivity ($\varepsilon_{\parallel}$, $\varepsilon_{\perp}$) measurements have been carried out for four different binary mixtures (x_{SF7} = 0.012, 0.03, 0.05 and 0.065) consisting of a hockey-stick shaped mesogen, 4-(3-decyloxyphenyliminomethyl) phenyl 4-decyloxycinnamate (SF7) and a calamitic compound 4′-octyloxy-4-cyanobiphenyl (8OCB). The molecular structures and transition scheme for both the compounds were discussed earlier in chapter 3. From the above measurement, different dielectric parameters such as temperature dependent dielectric anisotropy ($\Delta\varepsilon$) and average permittivity (ε_{avg}) have been determined for all the mixtures. Moreover, the critical exponent which defines the order nature of the *I-N* phase transition has also been extracted for all the studied mixtures by analyzing the pretransitional behavior of the average (ε_{avg}) and isotropic permittivity (ε_{Iso}) data. In addition,

the critical behavior in the vicinity of *N*–Sm-*A* phase transition has also been investigated to assess the order nature of the transition by extracting the value of critical exponent form the dielectric anisotropy data and then compared it with the same obtained from the high-resolution optical birefringence measurement [35]. Furthermore, a detailed study of the temperature-dependent splay elastic constant (K_{11}) [36-40], relaxation time (τ_0) as well as the rotational viscosity (γ_1) in the nematic phase for all the mixtures has been performed by capacitive decay method [25,41]. Additionally, the activation energy (E_a) has also been calculated with the help of rotational viscosity (γ_1) and order parameter ($<P_2>$) values, to make an idea about the intermolecular interaction.

4.2. Static dielectric parameter measurements

The temperature-dependent longitudinal and transverse component of the dielectric permittivity ($\varepsilon_{\parallel}$ and $\varepsilon_{\perp}$) has been measured in both planar and homeotropic configurations for four different mixtures by using Agilent 4294A LCR impedance analyzer. During cooling from a few degrees above the isotropic phase, the permittivity values have been acquired in the entire mesomorphic region. Additionally, the dielectric anisotropy ($\Delta\varepsilon = \varepsilon_{\parallel}-\varepsilon_{\perp}$) and also the average dielectric permittivity, $\varepsilon_{avg} = \{1/3(2\varepsilon_{\perp}+\varepsilon_{\parallel})\}$ values has been evaluated with the help of obtained parameters $\varepsilon_{\parallel}$ and $\varepsilon_{\perp}$. The variation of $\varepsilon_{\parallel}$, $\varepsilon_{\perp}$, ε_{avg} and $\Delta\varepsilon$ with respect to temperature at a constant frequency (10 kHz) are shown in Fig. 4.1(a-d) for all of the mixtures. It is evident from the figures that during cooling from the isotropic phase, the dielectric parameters $\varepsilon_{\parallel}$, $\varepsilon_{\perp}$ and $\Delta\varepsilon$ exhibit a sharp change on entering the *N* phase due to increase in orientational ordering. However, all the parameters reveal a small discontinuity in the vicinity of *N*–Sm-*A* phase transition which can be explained by considering a smectic-like short-range ordering developed within the nematic phase prior to the transition temperature. Interestingly, the value of longitudinal permittivity ($\varepsilon_{\parallel}$) at a specific temperature deep within the *N* or Sm-*A* phases has been found

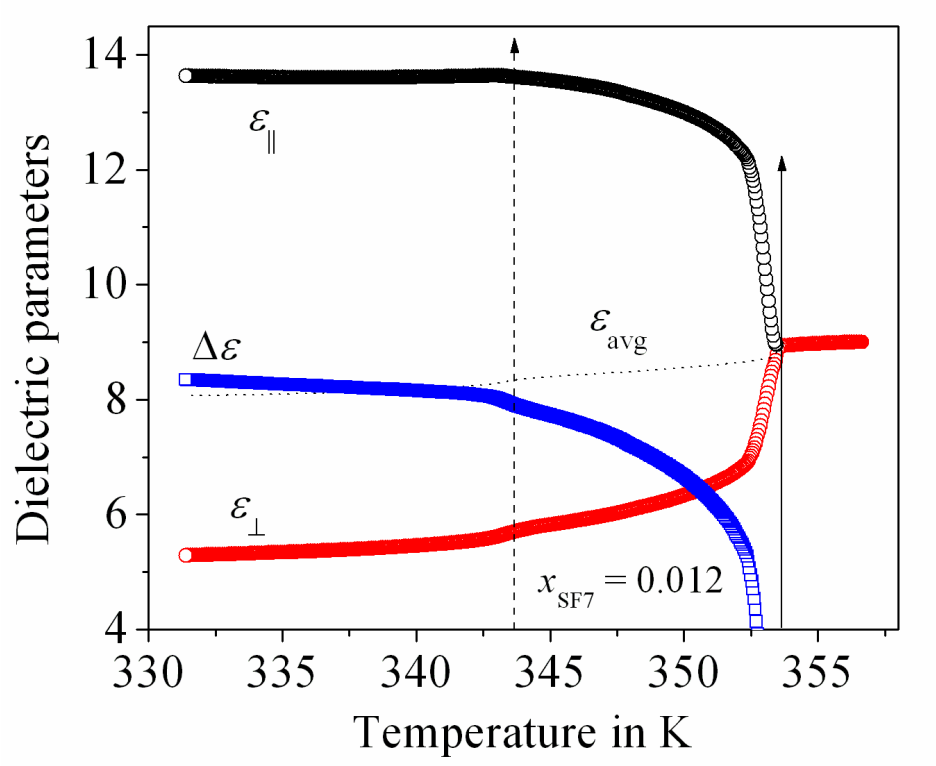

(a)

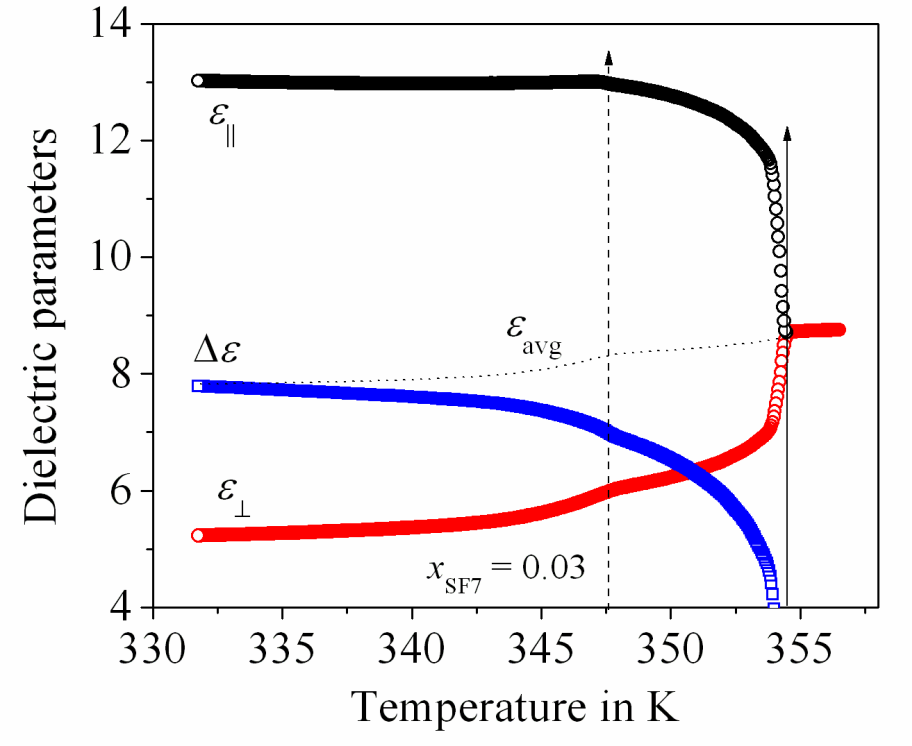

(b)

Figure 4.1. Temperature variation of the dielectric parameters for (a) x_{SF7} = 0.012 and (b) 0.03. Solid arrow and dashed vertical arrow indicate the *I*–*N* (T_{IN}) and the *N*–Sm-*A* (T_{NA}) phase transition temperatures respectively.

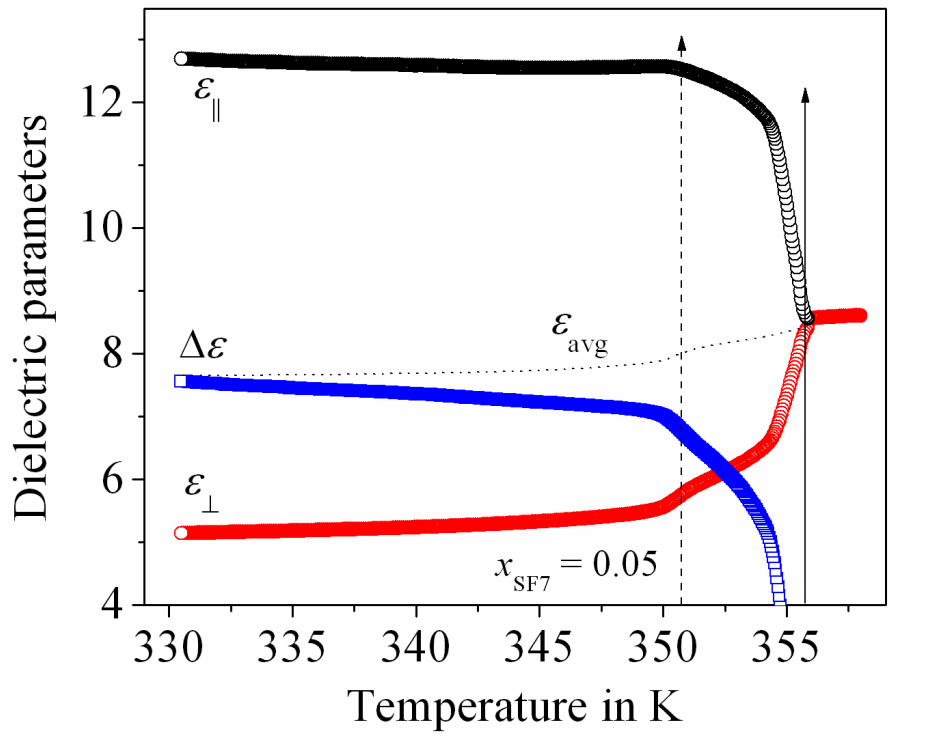

(c)

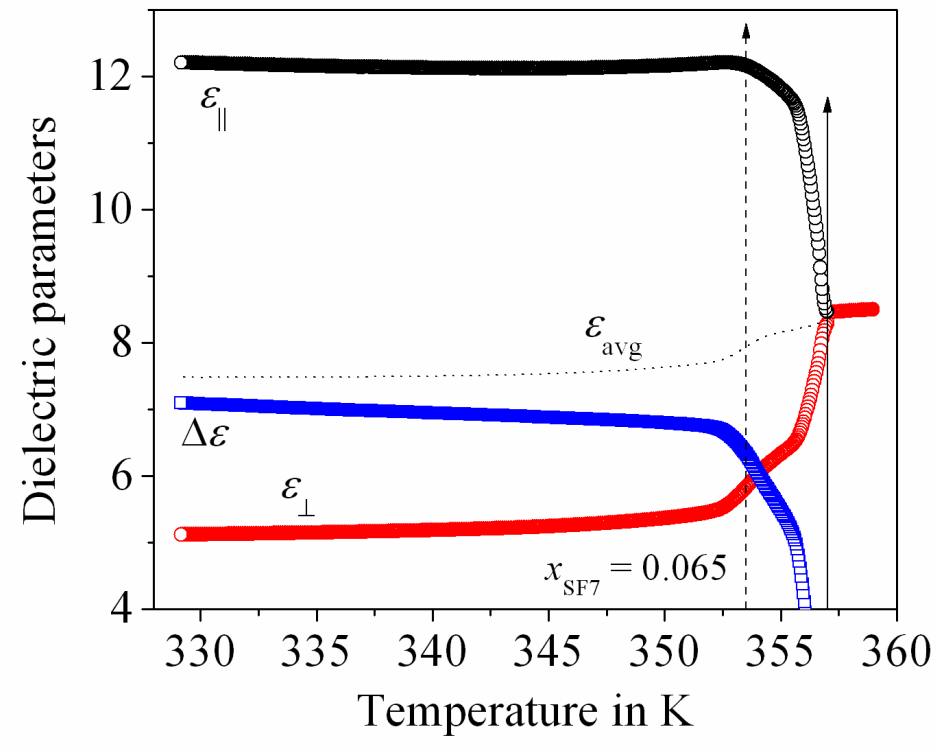

(d)

Figure 4.1 (cont'd). Temperature variation of the dielectric parameters for (c) x_{SF7} = 0.05 and (d) 0.065. Solid arrow and dashed vertical arrow indicate the *I*–*N* (T_{IN}) and the *N*–Sm-*A* (T_{NA}) phase transition temperatures respectively.

to be decreased with increasing the dopant concentration. It should be noted that the molecular structure of the pure calamitic compound 8OCB is made-up of a polar CN group attached to one end originating a strong polar nature of the molecule. Hence the compound 8OCB exhibits a large positive dielectric anisotropy ($\Delta\varepsilon$) throughout the mesophase region [42]. Again all the mixtures also possess a large positive dielectric anisotropy value in the *N* and Sm-*A* phases. However, by increasing the concentration of the hockey stick-shaped mesogen in the mixtures, the $\varepsilon_{\parallel}$ value and hence the $\Delta\varepsilon$ value gradually decreases as seen in Fig. 4.2. This phenomenon may be considered to be related with the effective value of dipole moment within the mixtures for the organization of both the dissimilar molecules. It can be assumed that a strong anti-parallel interaction between the molecular dipoles persuading a small

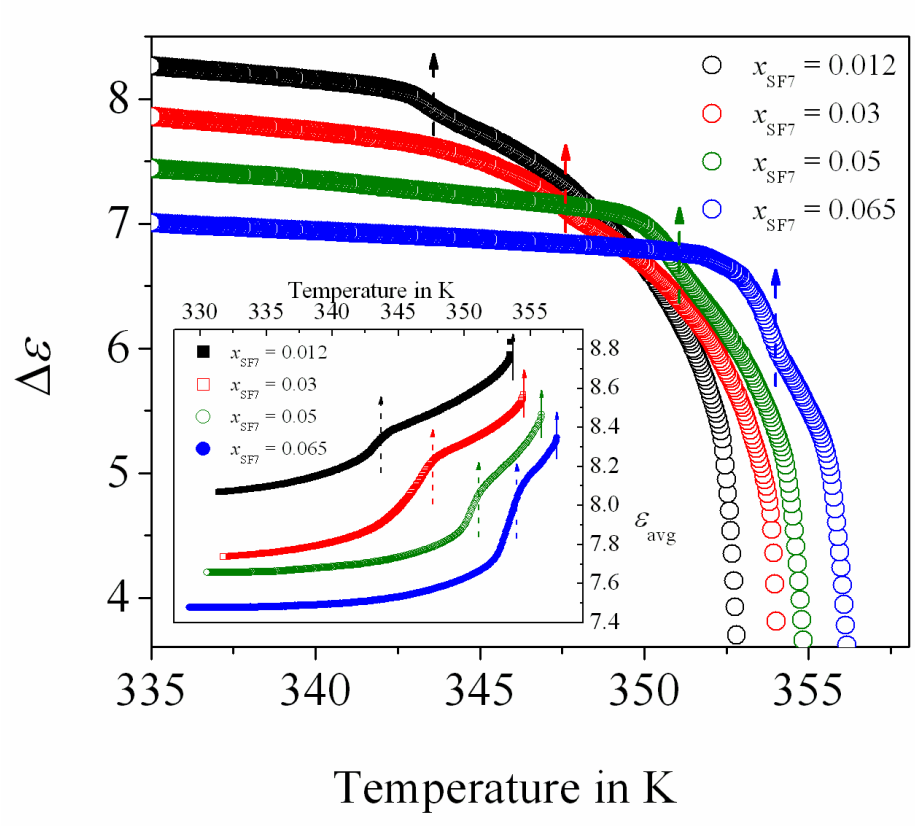

Figure 4.2. Temperature variation of the dielectric anisotropy ($\Delta\varepsilon$) for all the mixtures. Inset depicts the average permittivity (ε_{avg}) of the same. Solid arrow and dashed vertical arrow indicate the *I*–*N* (T_{IN}) and the *N*–Sm-*A* (T_{NA}) phase transition temperatures respectively.

reduction in the permittivity value [10,43] even for the presence of small amount of kink-shaped mesogen with 8OCB. Again this dipole-dipole interaction is quite strong in the nematic and smectic phases compared to that of the isotropic phase [44]. For this reason, the extrapolated value of isotropic permittivity (ε_{Iso}) in the nematic and smectic phases found to be relatively greater than the average permittivity (ε_{avg}) for all the investigating mixtures. However, this difference (ε_{iso}- ε_{avg}) increases as the concentration of the hockey stick-shaped compound increases which is clearly visible in the representative curves of ε_{avg} (inset of Fig. 4.2) in both the nematic and smectic phases.

In order to investigate the pretransitional behavior in the vicinity of *I–N* phase transition and to extract the critical exponent related with the fluctuation at this transition, the temperature dependent permittivity data has been suitably used. The study of the pretransitional effect in the vicinity of *I–N* phase transition has been reported earlier in several pure calamitic compounds [45-49] as well as in some binary mixtures of calamitic compounds [44] and also has been described in the hockey stick-shaped compound [50]. Therefore, it is quite interesting to investigate the pretransitional phenomena in the mixtures of compounds having divergent molecular conformer. During the past few decades, the mean field model cannot describe the exact experimental observations based on the linear and non-linear dielectric permittivity studies. Therefore, a fluid-like model [51,52] has been considered to explain the pretransitional behavior at that transition. According to this model, the permittivity can be well described by the fluid like equation [52-56]:

$$\varepsilon_{\text{Iso}}(T) = \varepsilon^{*} + A_1^{+}(T - T^{*}) + A_2^{+}(T - T^{*})^{1-\alpha''} \qquad (4.1)$$

For $T > T_{IN} = T^{*} + \Delta T^{*}$

$$\varepsilon_{\text{avg}}(\text{T}) = \varepsilon^{**} + A_1^{-}(T^{**} - T) + A_2^{-}(T^{**} - T)^{1-\alpha''} \qquad (4.2)$$

For $T < T_{IN} = T^{**} - \Delta T^{**}$

where, ε^{*} and ε^{**} are the dielectric permittivity values (ε_{Iso} and ε_{avg} respectively) at the critical temperatures T^{*} and T^{**} (extrapolated temperature of virtual

continuous phase transition) respectively. Here α'' is the critical exponent similar to the specific heat capacity critical exponent α and A_1^+, A_1^-, A_2^+ and A_2^- are the critical amplitudes.

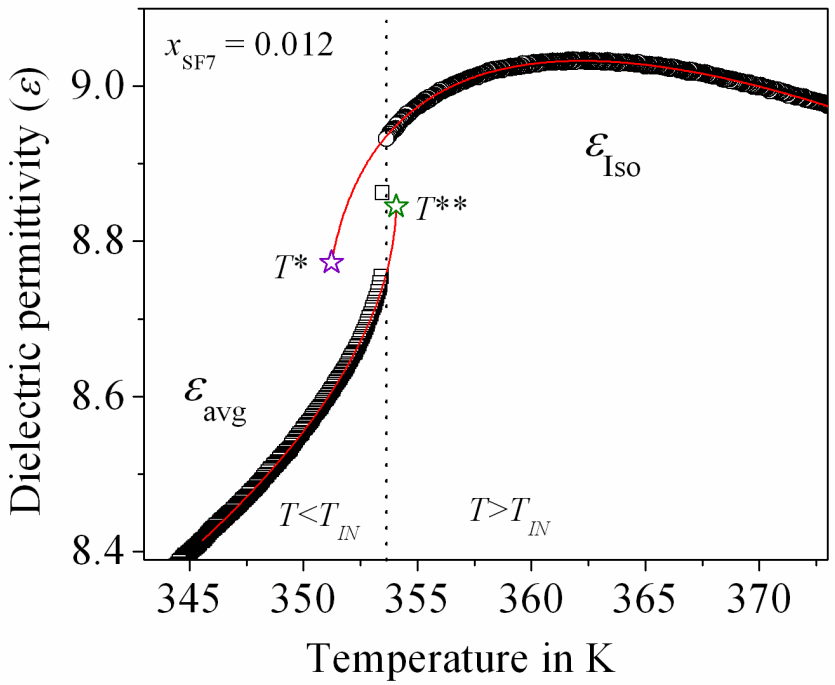

Figure 4.3. Variation of permittivitties with temperature for the concentration x_{SF7} = 0.012. Solid lines are fit to Eq. (4.1) and (4.2). The critical temperatures T^* and T^{**} are indicated with star symbols (☆) and the dotted vertical line represents the nematic-isotropic phase transition temperature (T_{IN}).

In the present investigation, all the mixtures were heated up to 25-30 K above the clearing temperature and the permittivity values has been measured during cooling at a rate of 0.5 K per minute with a fixed frequency 10 kHz. The above mentioned Eq. (4.1) and Eq. (4.2) were fitted to the experimental data points of permittivity in the isotropic phase (ε_{Iso}) as well as in the nematic phase (ε_{avg}) individually, *i.e.*, above and below the clearing temperature (T_{IN}). The best-fitted parameters are shown in Table 4.1. One of the fit representation is shown in Fig. 4.3 for the mixture x_{SF7} = 0.012 in both the isotropic and nematic phases. Moreover, the temperature variations of ε_{Iso} for all the studied mixtures are displayed in Fig. 4.4 in accordance with the fitted curve to Eq. (4.1).

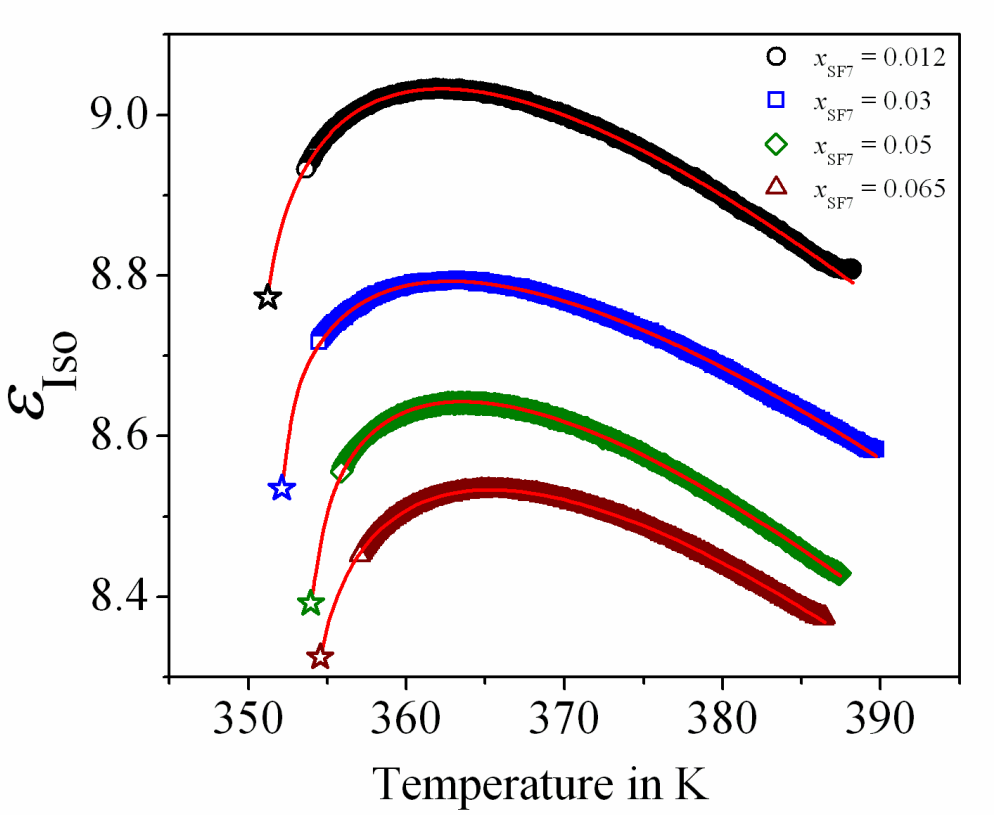

Figure 4.4. Variation of the isotropic permittivity (ε_{Iso}) with temperature for all of the mixtures. Solid lines are the fit to Eq. (4.1) and the star symbols (☆) are representing the critical temperatures (T^*).

The observation made from Fig. 4.3 and 4.4 that the isotropic permittivity (ε_{Iso}) follows a bending pattern after attaining a maximum value for all the mixtures and the value of ε_{Iso} is greater than the value of ε_{avg} in the neighborhood of the clearing temperature. However, at very close to the clearing temperature (T_{IN}), the value of ε_{Iso} sharply decreases as the temperature decreases, exhibiting a strong pretransitional behavior. This pretransitional behavior is originating due to the pre-nematic fluctuations of the pseudo nematic clusters developed within the isotropic phase. Moreover, the amount of bending decreases as the dopant concentration increases. It should be noted that the calamitic compound 8OCB has a greater dipole moment (6.3 D, along its long axis) in comparison to the dopant (4.48 D) having divergent molecular structure. The mutual anti-parallel interaction of the dipoles effectively

minimizes the resultant dipole moment in the mixture with a reduction in the pretransitional effect for the investigated systems. The observation of such pretransitional phenomena has also been confirmed by others in case of pure compound as well as in binary mixtures [44,56,57]. It has been claimed that owing to the existence of polar terminal groups, the adjacent molecules prefer to figure out an anti-parallel pair to reduce the effective dipole moment within the mesogenic system [58,59]. This anti-parallel packing originating the pseudo clusters within the medium. Thus the amount of bending and associated permittivity value in the isotropic phase decreases with increasing the hockey-stick shaped molecular concentration. Furthermore, a relative competition between the parallel and anti-parallel components of the dipole moment takes place near the *I-N* phase transition temperature. In the locality of T_{IN}, the anti-parallel component dominates and exhibiting a critical behavior.

Table 4.1. Results corresponding to the best fit for permittivity above and below the isotropic-nematic (T_{IN}) phase transition temperatures obtained in accordance with Eq. (4.1) and Eq. (4.2).

x_{SF7}	Condition	T^* / T^{**} (K)	ε^* or ε^{**}	A_1^+ or A_1^-	A_2^+ or A_2^-	α''
0.012	$T>T_{IN}$	351.230±0.230	8.721±0.009	-0.031±0.001	0.193±0.001	0.494±0.011
	$T<T_{IN}$	354.271±0.191	8.803±0.024	-0.029±0.010	-0.116±0.014	0.500±0.002
0.03	$T>T_{IN}$	353.103±0.078	8.511±0.019	-0.026±0.001	0.173±0.012	0.502±0.022
	$T<T_{IN}$	354.608±2.057	8.591±0.213	-0.025±0.007	-0.117±0.105	0.499±0.281
0.05	$T>T_{IN}$	354.184±0.002	8.374±0.004	-0.030±0.001	0.176±0.003	0.49±0.008
	$T<T_{IN}$	355.876±1.379	8.485±0.170	-0.031±0.004	-0.119±0.069	0.499±0.118
0.065	$T>T_{IN}$	354.000±0.085	8.190±0.022	-0.030±0.001	0.204±0.014	0.500±0.022
	$T<T_{IN}$	357.175±1.859	8.390±1.805	-0.029±0.020	-0.115±0.732	0.498±0.051

An inspection of Table 4.1 reveals that the extracted α'' values lie in between 0.49±0.008 and 0.502±0.022, indicating a tricritical nature of the *I–N* phase transition. These results agree well with the predicted critical exponent

value from tricritical hypothesis (α_{TCH} = 0.5) [60-62]. Furthermore, an insight into the other parameters shows that $|A_2^+/A_2^-|$ value lies in a range from 1.47 to 1.77, whereas the $|A_1^+/A_1^-|$ value is nearly or slightly greater than unity but have no systematic variation on increasing the molar concentration. A finite measurable difference between T^* and T^{**} has also been detected and both of them also differ from the value of T_{IN}. Therefore, the relative deviation for both of $T^*$and T^{**} with respect to the *I–N* phase transition temperature ($\Delta T^* = T_{IN} - T^*$, $\Delta T^{**} = T^{**} - T_{IN}$), along with the metastable region (T^{**}-T^*) can be easily assumed from Table 4.1. However, no systematic variation has been recognized of them with the variation of dopant concentration.

4.3. Critical behavior at the *N*−Sm-*A* phase transition

The anisotropy data of any physical parameter can be treated as an order parameter of the system, which is the elementary essence for analyzing the critical fluctuation associated with a transition. In chapter 3, the optical birefringence (Δn) data has been successfully employed to investigate the critical behavior in the vicinity of *N*−Sm-*A* phase transition, while in the present case the dielectric anisotropy data ($\Delta\varepsilon$) is being used as another observable order parameter for the same LC binary system. Similar to the optical birefringence (Δn) data, the dielectric anisotropy ($\Delta\varepsilon$) data also does not manifest any noticeable discontinuity at the *N*−Sm-*A* phase transition, but the main difference in both of Δn and $\Delta\varepsilon$ data for the pure compound and for the mixtures lie in the vicinity of the *N*−Sm-*A* phase transition as being observed from Fig. 4.2. Hence a quantity E(*T*) similar to Q(*T*) in chapter 3, has been considered in this case to study the critical anomaly associated with that transition and can be expressed as [63,64]:

$$\mathrm{E}(T) = -\frac{\Delta\varepsilon(T) - \Delta\varepsilon(T_{NA})}{T - T_{NA}} \qquad (4.3)$$

where $\Delta\varepsilon(T_{NA})$ is the dielectric anisotropy value at the *N*–Sm-*A* transition temperature (T_{NA}). In order to characterize all the parameters, E(T) has been fitted with the power-law expression (similar to Eq. (3.7) in chapter 3):

$$\mathrm{E}(T) = A^{\pm}|\tau|^{-\alpha'}(1 + D^{\pm}|\tau|^{\Delta}) + C(T - T_{NA}) + B \qquad (4.4)$$

where, τ = (T-T_{NA})/T_{NA} is the reduced temperature, α' is the effective critical exponent similar to specific heat capacity critical exponent α.

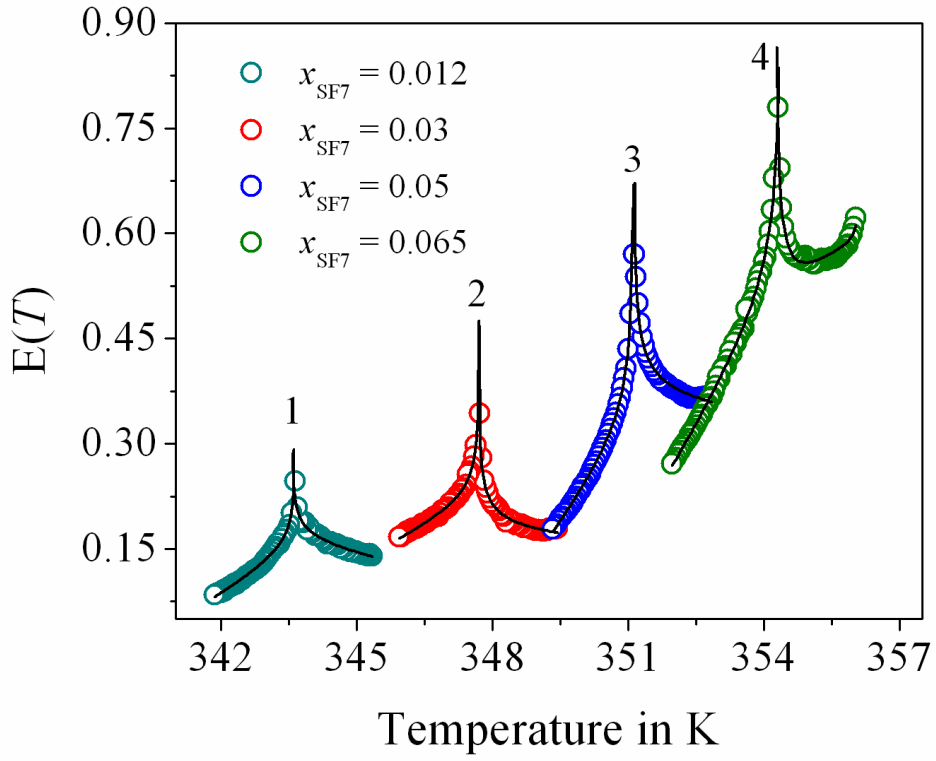

Figure 4.5. Temperature-dependent variation of the quotient E(T) in the vicinity of *N*–Sm-*A* phase transition at different mole fractions of SF7 in the binary mixtures. The solid lines are fit to Eq. (4.4).

In the present analysis, the reduced temperature (τ) value has been taken as fixed at 5×10^{-3} for all of the mixtures in both the *N* and Sm-*A* phases and Δ value is also set fixed at 0.5 without any further variation. A representative variation of E(T) with temperature has been illustrated in Fig. 4.5 along with a fitting line of Eq. (4.4) for all the mixtures. The extracted parameter values are listed in Table 4.2 along with a reduced error function χ_v^2.

Table 4.2. Results corresponding to the best fit for E(*T*) near *N*−Sm-*A* phase transition obtained in accordance with Eq. (4.4) and related χ_v^2 values associated with the fits. $|\tau|_{max}$ presents the upper limit of reduced temperature considered for these fits.

x_{SF7}	α'	A^-/A^+	D^-/D^+	$\|\tau\|_{max}$	χ_v^2
0.012	0.273±0.037	0.972±0.112	0.988±0.003	5×10^{-3}	1.51
0.03	0.389±0.029	1.010±0.071	1.003±0.023	5×10^{-3}	1.35
0.05	0.439±0.017	1.184±0.028	1.008±0.091	5×10^{-3}	1.13
0.065	0.489±0.021	1.475±0.374	1.182±0.049	5×10^{-3}	1.22

An inspection of Fig. 4.5 reveals that as the concentration increases, the peak height of E(*T*) in the vicinity of *N*−Sm-*A* phase transition systematically increases and achieve a maximum value in the present investigating system for the mixture with the highest concentration (x_{SF7} = 0.065). Moreover, the effective critical exponent α' is found to lie in a range between 0.273±0.037 and 0.489±0.021 with a reasonable χ_v^2 value in between 1.13 and 1.51. Fig. 4.6(a-b) representing the variation of the effective critical exponent α' against the concentration of hockey stick-shaped mesogen and also with the variation of McMillan ratio respectively. A comparison has also been done for the extracted α' value with the same obtained from optical anisotropy (Δn) data reported in chapter 3. Fig. 4.6(a-b) clearly shows that the yielded α' values from both the experimental data of Δn and $\Delta\varepsilon$ are almost identical. Moreover, they are limited in between the 3D-*XY* (α' = -0.007) and TCP (tricritical point; α' = 0.5) [35,65]. Additionally, the quotient A^-/A^+ shows an increasing pattern from 0.972 ± 0.112 for x_{SF7} = 0.012 to 1.475 ± 0.374 for x_{SF7} = 0.065, whereas D^-/D^+ values remain more or less equal to unity which are also found to be in accordance with the theoretical hypothesis. Accordingly, a non-universal behavior of the effective critical exponent α' has been observed and hence it defines a crossover character from second order to first order nature of the

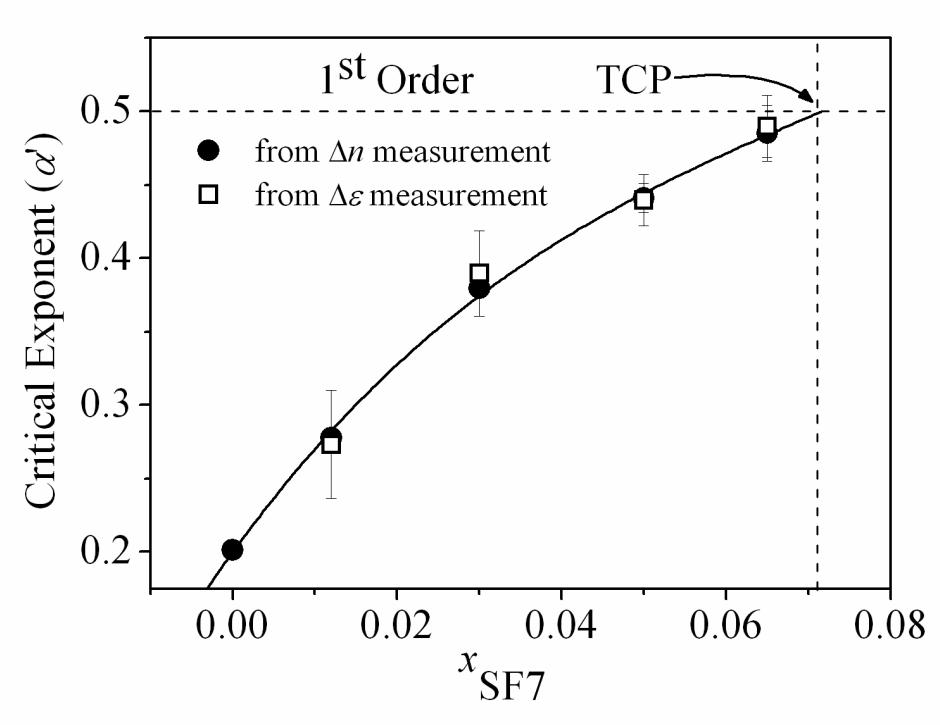

(a)

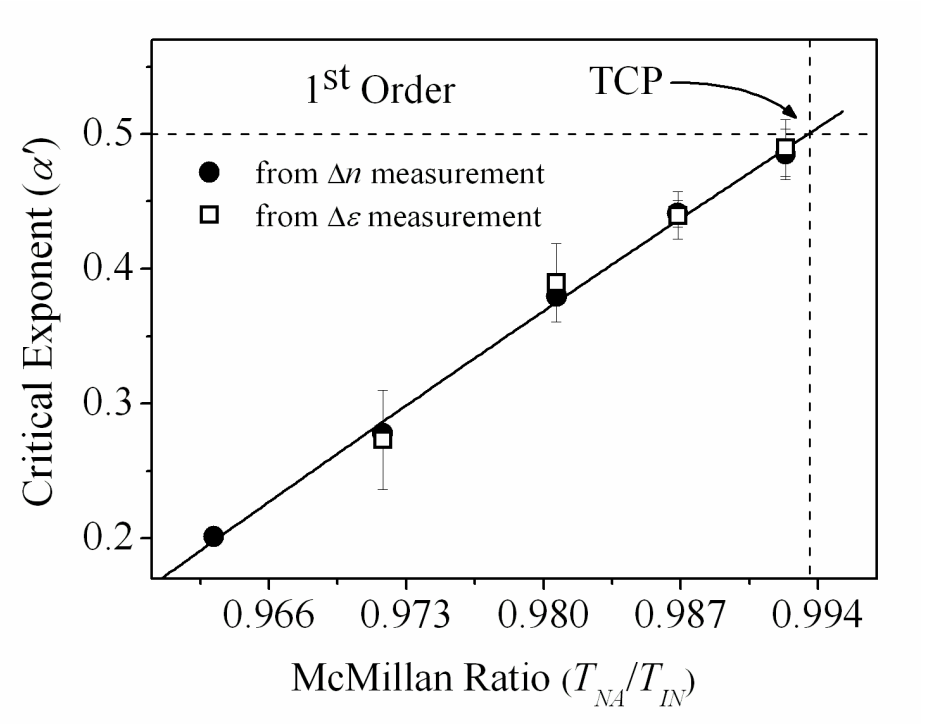

(b)

Figure 4.6. The variation of the effective critical exponent (α') with (a) molar concentration and (b) McMillan ratio (T_{NA}/T_{IN}), obtained by fitting E(T) to Eq. (4.4). The vertical dashed line corresponds to the tricritical point (TCP). The solid lines are the polynomial fits to the data points.

N−Sm-*A* phase transitions in the present investigated mixtures. Analytically this crossover point has been found for a composition $x_{SF7} \sim 0.072$ with $\alpha' = 0.5$ and the corresponding McMillan ratio (*i.e.*, T_{NA}/T_{IN}) is being ~ 0.994. Therefore, as an additive, the role of the compound SF7 in the mixture is reflected by a substantial change in the width of the nematic phase which further drives the second order *N*−Sm-*A* phase transition towards the first order in nature. Indeed these results are found to be well consistency with the same obtained by investigating the high-resolution optical birefringence (Δn) data in a quite identical procedure presented in chapter 3.

4.4. Threshold voltage and splay elastic constant measurements

Due to the application of sufficient electric field to a planar aligned mesogenic medium in an orthogonal direction to the molecular long axis, the Freedericksz transition [36,37] takes place within the system, resulting a rotation of the molecular directors along the field direction. Beyond this Freedericksz threshold voltage (V_{th}), the capacitance value ($C_{\perp}$) for planar aligned sample sharply increases up to a saturation value ($C_{||}$). However, these V_{th} and $C_{||}$ both are depends upon the sample temperature. In the present investigated mixtures, the voltage-dependent capacitance value has been measured only in the nematic phase by using Agilent 4980A. A representative *C*-*V* diagram is displayed in Fig. 4.7 for a mixture having molar concentration $x_{SF7} = 0.012$ at different temperatures in the nematic phase and a few degrees below the *N*–Sm-*A* phase transition temperature. The value of V_{th}'s can be easily achieved from these curves. Fig. 4.8 depicts the temperature variation of V_{th} in the nematic phase for four different concentrations. It is clearly observed that by decreasing the temperature, the value of V_{th} gradually increases over the nematic phase due to an enhancement of orientational ordering as well as of molecular packing. All the mixtures follow more or less same variation by reducing the temperature. However, a noticeable increasing pattern has been

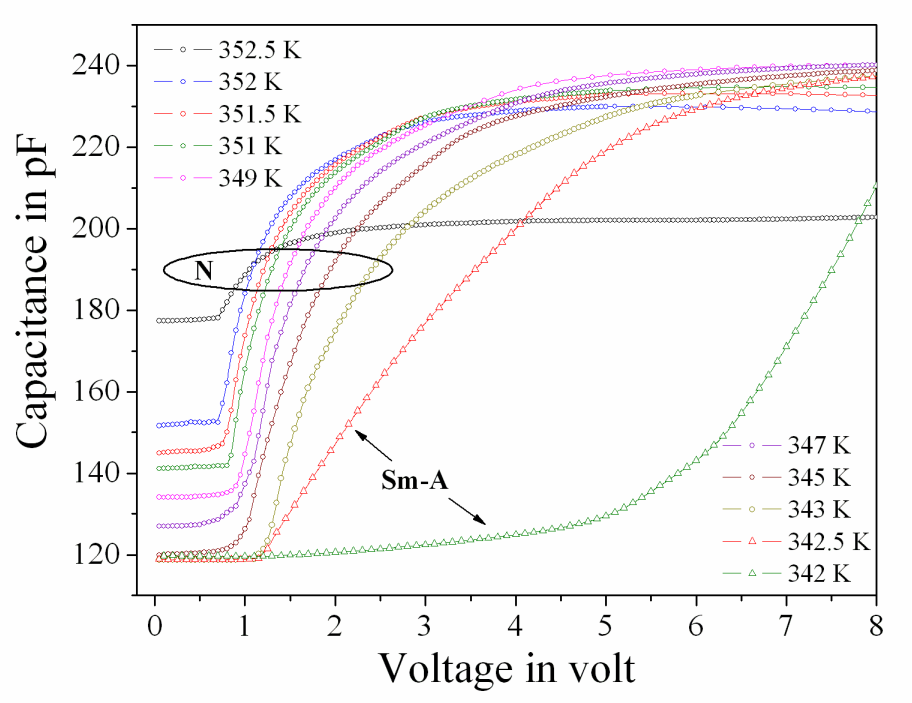

Figure 4.7. Variation of cell capacitance in planar configuration at different temperatures for x_{SF7} = 0.012. Different temperatures are mentioned in the figure in unit of Kelvin (K).

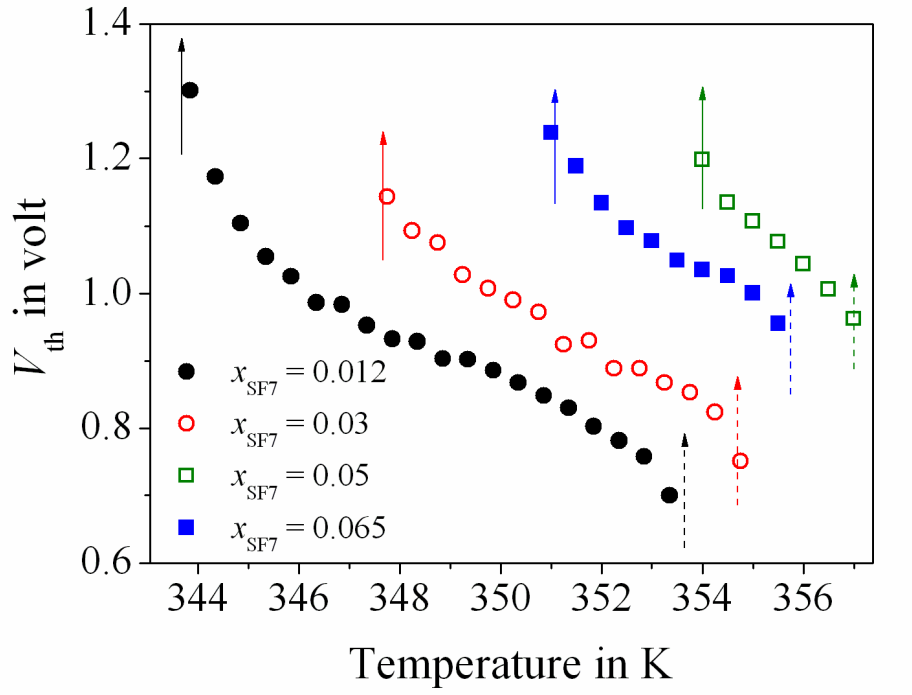

Figure 4.8. The variations of threshold voltage (V_{th}) with temperature for all the mixtures only in nematic phase. The vertical dashed line and solid line corresponds to the T_{IN} and T_{NA} respectively for each of molar concentration.

found in the value of V_{th} with increasing the dopant concentration, implying that the strength of the electric field required to reorient the director axis becomes larger for the mixtures of higher concentrations. As an effect of increasing the kink-shaped mesogen, the molecular packing increases within the medium and an additional hindrance is developed to the molecular switching owing to the presence of bend-angle of the SF7 molecule. Additionally, the molecules have a tendency to lowering the orientational ordering within the nematic phase as well as for the stiffness of the molecules a short-range smectic-like ordering seems to be developed in higher concentrations which plays an important role in diminishing the nematic range and enhancing the value of V_{th}.

The splay elastic constant (K_{11}) has been determined in the nematic phase for all the investigating binary mixtures with the help of obtained value of the threshold voltage (V_{th}) and the dielectric anisotropy ($\Delta\varepsilon$) using the following relation [31,66-68]:

$$K_{11} = \frac{\varepsilon_0 \Delta\varepsilon V_{th}^2}{\pi^2} \tag{4.5}$$

where ε_0 is the free space permittivity. Fig. 4.9 represents the variation of K_{11} as a function of reduced temperature (T-T_{IN}). In this figure, K_{11} demonstrates a gradual increase in magnitude from ~0.2 pN to a maximum value ~10 pN (for x_{SF7} = 0.012) throughout the entire mesophase with lowering the temperature. This is the common phenomena seen for both rod-like and bent-core mesogens. All of the investigated mixtures possess the same increasing pattern but the slope of this variation gradually increases with increasing the amount of the hockey stick-shaped mesogen. However, each of these curves exhibits a pretransitional behavior on approaching the *N*–Sm-*A* phase transition temperature. Probably some small domains with strong short-range smectic-like ordering of the molecules developed within the nematic phase which is being extended further during cooling, exhibiting such behavior at very close to

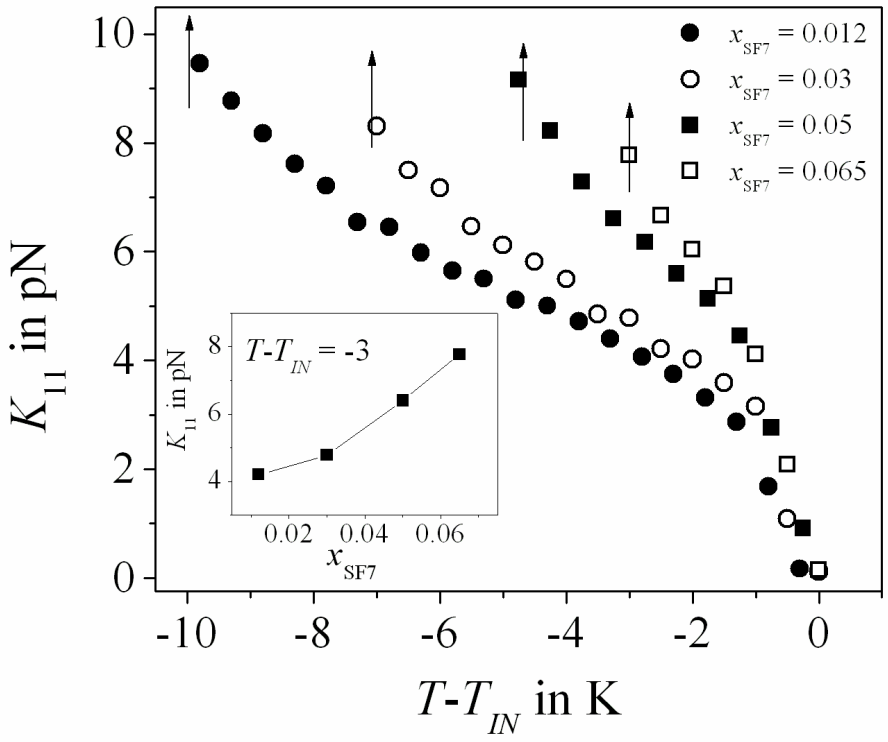

Figure 4.9. The variation of the splay elastic constant (K_{11}) with reduced temperature for all the mixtures in the nematic phase. The vertical arrows correspond to T_{NA} for each of molar concentration.

the transition temperature. A number of pure calamitic compounds as well as their mixtures [67,69-71] also suggesting similar type of pretransitional phenomena. Conversely, some of the bent-core [72-74] and hockey stick-shaped compounds [29] were found not to demonstrate any pretransitional divergence of K_{11}. Here in this case also for the mixture x_{SF7} = 0.012 in which the amount of hockey stick-shaped dopant is quite small, a prominent pretransitional effect is visible, while it is not so evident in mixtures of higher concentrations. The magnitude of the splay elastic constant for the lower concentration is very close to the reported value of the same for pure compound 8OCB [26,75]. Due to the combined effect of a relatively higher value of dielectric anisotropy ($\Delta\varepsilon$) and a lower value of threshold voltage (V_{th}) leads to a smaller value of elastic constant for the mixture x_{SF7} = 0.012 well within the nematic phase. Further increase in the dopant concentration, K_{11}

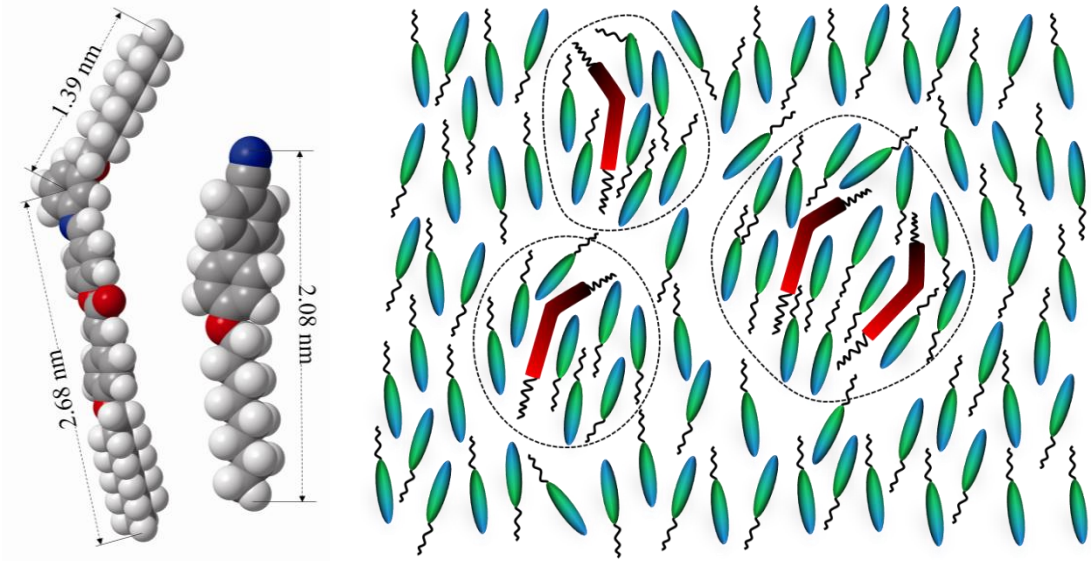

(a) (b)

Figure 4.10. (a) Energy optimized molecular structure of SF7 and 8OCB. (b) Mutual alignment of both the hockey-stick shaped (SF7) and calamitic molecule (8OCB) in the nematic phase.

value reveals a monotonic enhancement at a particular temperature say $|T_{IN} - T| = 3$ (inset of Fig. 4.9), although the value of K_{11} for all cases coalesces near the clearing temperature ($T_{IN} - T = 0$). The above observation can be explained by considering the mutual orientation of the molecules in the mixture, creating a frustration in the molecular packing of calamitic mesogen (8OCB) by the hockey-stick shaped compound (SF7). The host calamitic molecule has a length 2.08 nm, while the longer part of the hockey stick-shaped mesogen (SF7) is about 2.68 nm along with a shorter arm of length 1.39 nm (see Fig. 4.10(a)). It is believed that owing to the affinity to form pair production of the polar groups, the calamitic molecules prefer to align themselves parallel to the longer arms of the hockey stick-shaped mesogen. As a result of such organization, a number of small sized temporary clusters (see Fig. 4.10(b)) are formed within the nematic phase and for the anti-parallel interactions of the dipoles effectively reduces the polar contribution along the director. Effect of such decrease in mutual dipole moment reflected by a relatively lower value of $\Delta\varepsilon$ compared to the pure compound. Moreover, the efficient packing of two

dissimilar molecules remarkably restricts the splay deformation. Earlier reports in binary mixtures of calamitic and bent-core compounds [58,59] also favor such type of molecular packing in the nematic phase representing a monotonic enhancement of K_{11} with increasing the bent-core mesogens within the mixture. Furthermore, the mutual alignment of both dissimilar molecules in the present system leads to a decrease in the nematic width. The smectic-like short range ordering developed within the clusters represents an intrinsic part of the nematic phase efficiently increases near the *N*–Sm-*A* phase transition which in turn rapidly enhances the value of the splay elastic constant.

4.5. Relaxation time and rotational viscosity measurements

Using the capacitive decay technique [25,41], the molecular relaxation time (τ_0) has been determined for all the mixtures over the entire nematic phase. A systematic variation of relaxation time (τ_0) with reduced temperature

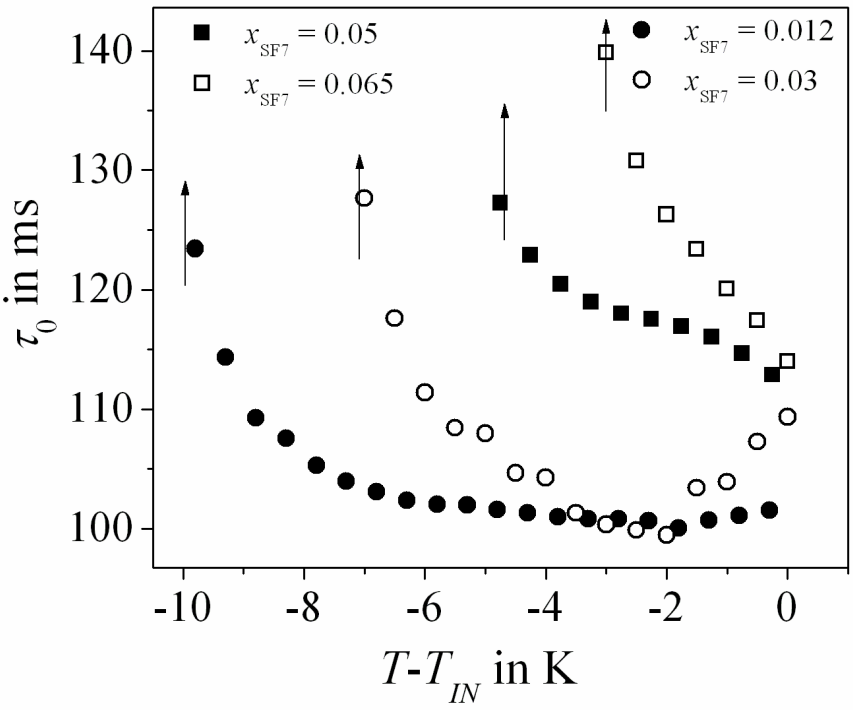

Figure 4.11. The variation of the relaxation time (τ_0) with reduced temperature for all the mixtures in the nematic phase. The vertical arrows correspond to T_{NA} for each of molar concentration.

is shown in Fig. 4.11. It is quite evident that during cooling from the isotropic phase, τ_0 value increases from ~100 ms to a maximum value ~124 ms for the lower concentration (x_{SF7} = 0.012) which is possibly due to increase in the orientational ordering within the nematic phase. Moreover, in the vicinity of *N*–Sm-*A* phase transition it exhibits a sharp augmentation. Further increase in the dopant angular mesogenic concentration, τ_0 values are also found to enhance progressively at a particular temperature (T_{IN}-T) well within the nematic phase. A greater intermolecular packing of two dissimilar molecules existing in the mixtures and also for the influence of bending feature of SF7 molecule considerably hinders the rotational motion of the molecules within the system and renders an increasing trend of τ_0 value.

Rotational viscosity plays a significant role to determine the dynamical behavior of molecules within the LC system. In the present binary system, the value of rotational viscosity (γ_1) has been measured using the following relation [25,31,41]:

$$\gamma_1 = \frac{\tau_0 K_{11} \pi^2}{d^2} \tag{4.6}$$

where d is the thickness of the planar-aligned LC cell and τ_0, K_{11} are the relaxation time and splay elastic constant respectively, those are already measured. The variation of rotational viscosity (γ_1) with reduced temperature has been depicted in Fig. 4.12 for all the investigated mixture over the entire nematic phase. As the value of γ_1 is directly proportional to the value of K_{11}, the divergence of γ_1 has found to be in agreement with that of K_{11}, *i.e.*, the value of γ_1 increases monotonically by reducing the temperature and finally assumes a maximum value on approaching the *N*–Sm-*A* phase transition temperature. This is due to the gradual enhancement of the molecular orientational ordering throughout the nematic range. A quite similar type of observation has been reported in some pure bent-core systems [25,31] as well as in a mixture of bent-core and calamitic LC molecules [76,77]. However, all the mixtures exhibit a pretransitional behavior in the vicinity of *N*–Sm-*A* phase transition

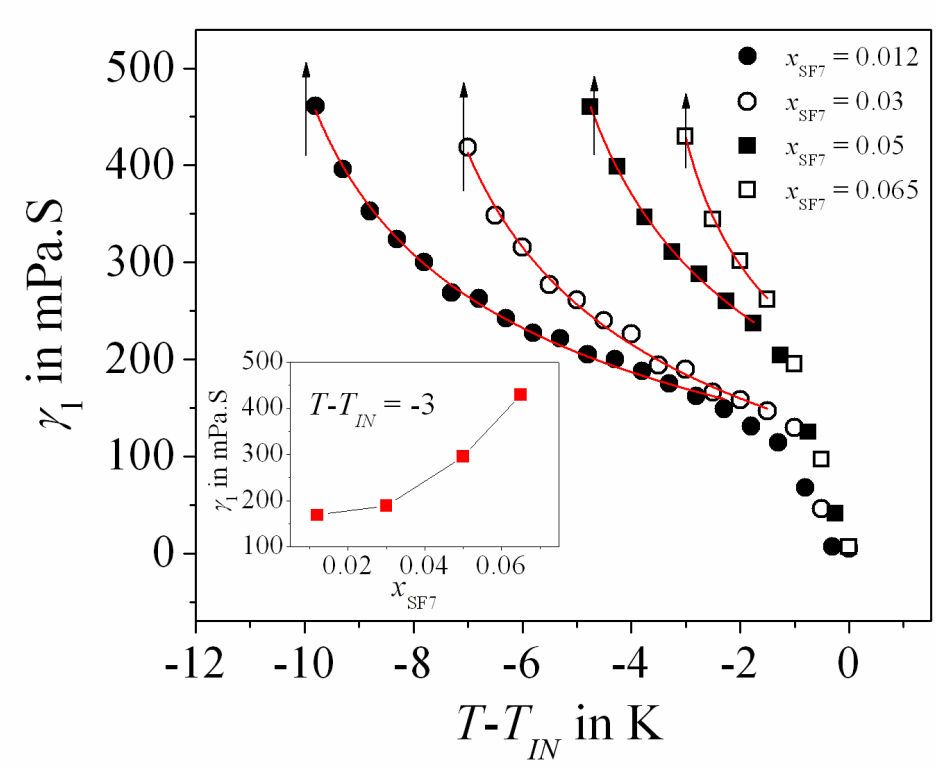

Figure 4.12. The variation of rotational viscosity (γ_1) with reduced temperature for all the mixtures only in nematic phase. The vertical arrows correspond to T_{NA} for each of molar concentration. Solid lines are fit to Eq. (4.7).

because of the short-range smectic fluctuations in the nematic phase. Interestingly, the slope of the monotonic enhancement becomes higher by increasing the hockey stick-shaped compound within the mixtures. This implies that for a particular temperature say $|T_{IN}-T|$ = 3, the value of γ_1 increases with increase in concentration of hockey stick-shaped mesogen as depicted in inset of Fig. (4.12). In general the usual rod-like compounds possess a temperature dependent lower value of the rotational viscosity (γ_1) in the nematic phase [78-80], while it has been reported to assume a relatively higher value in bent-core compounds [29-31]. Dorjgotov *et al.* [30] reported that the value of γ_1 is much higher (10 times) for the bent-core LC compound having negative dielectric anisotropy than usual calamitic systems, whereas Satyanarayana *et al.* [31] has proposed slightly larger value of γ_1 for a pure bent-core system having positive dielectric anisotropy. Therefore, it is expected and indeed experimentally proved that the present investigated binary system assumes a value of γ_1

between that of a typical calamitic compounds (here 8OCB) and certain higher value of the bent-core mesogens. Such type of increasing character has also been reported earlier in some binary mixtures of calamitic and bent-core compounds [58,77]. The well-organized packing of dissimilar molecules within the temporary clusters (Fig. 4.10(b)) possesses a strong transverse polar interaction due to the presence of kink-shaped molecules and thereby represents a slightly higher value of γ_1. However, the yielded values of γ_1 in the mixtures have found slightly higher than that of the pure 8OCB compound [80]. The hockey stick-shaped molecule (asymmetric bent-core) used in the present binary system (bending angle = 109.1^o) differs significantly from the typical bent-core compounds. Therefore, the effective values of rotational viscosity of the present binary system consisting of a hockey stick-shaped mesogen are found to be intermediate between the typical bent-core compounds and usual calamitic compounds. Moreover, due to the influence of smectic-like short-range fluctuation within the aggregates or clusters as well as for the increase of order parameter in the nematic phase, a rotational hindrance has been experienced by the molecules [81]. By lowering the temperature, the size of the temporary clusters rapidly grows up within the nematic phase which further causes a clear pretransitional behavior of the rotational viscosity (γ_1) data (Fig. 4.12). In an attempt to investigate such pretransitional behavior associated with the rotational viscosity (γ_1) data in the vicinity of *N*–Sm-*A* phase transition the critical exponent (ν) has been analyzed using the following relation [82,83]:

$$\gamma_1 = \mathrm{a}(T - T_{NA})^{-\nu} + \mathrm{b} \qquad (4.7)$$

where a and b are two fit parameters and T_{NA} is the *N*–Sm-*A* phase transition temperature. Fit parameters are displayed in Table 4.3 and fitted lines are also displayed in the same figure as red lines for all the mixtures. According to mean field theoretical model of McMillan [84] the critical exponent (ν) assume a value 0.5, while by considering a local rotation of the director and the smectic

Table 4.3. Fit parameters obtained from the fitting of the temperature dependence of γ_1 to Eq. (4.7) for different molar concentrations.

x_{SF7}	a	b	ν
0.012	819.09±1.55	-234.95±2.33	0.33±0.01
0.03	856.57±3.85	-294.29±1.98	0.33±0.03
0.05	875.52±3.01	-272.76±2.52	0.34±0.19
0.065	550.65±1.15	-139.11±3.16	0.35±0.04

layers in the clusters, Jähnig *et al.* [82] have found this value nearly equal to 0.33. The extracted critical exponent (ν) value obtained by fitting the temperature dependent γ_1 value with Eq. (4.7) is found to lie between 0.33 and 0.35 within the error limit for different concentrations studied here. Hence, the extracted critical exponent values are almost in agreement with (ν = 0.33) the value proposed by Jähnig *et al.* [82] and therefore excluding the higher possible mean field value (ν = 0.5).

4.6. Determination of activation energy

Activation energy (E_a) makes an idea about the potential hindrance occurs due to the local field generated by other molecules in the system against which the director rotates. It suggests the knowledge about molecular mechanics, *i.e.*, inter-molecular packing and their interaction. The activation energy (E_a) strongly depends upon molecular order parameter $<P_2>$, rotational viscosity (γ_1) and can be obtained by the relation [85-88]:

$$\gamma_1 = \gamma_0 < P_2 > \exp\left(\frac{E_a}{k_\beta T}\right) \tag{4.8}$$

where k_β is the Boltzmann's constant and $<P_2>$ is the orientational order parameter which has been obtained for all of the above concentrations by analyzing optical birefringence data from high-resolution optical transmission measurement.

In an attempt to obtain the temperature variation of the orientational order parameter (<P_2>), the high-resolution optical birefringence (Δn) data as reported in Chapter 3 has been suitably used for all the mixtures under study. According to de Gennes [89], the anisotropy of any physical quantity can be a measure of orientational order parameter which provides a value in between 0 for a completely disordered phase and 1 for a completely ordered phase. As suggested by several workers [90-94], the optical anisotropy, *i.e.*, the birefringence (Δn) value can be adopted for the determination of the order parameter because the thermal variation of Δn provides useful information regarding the order of the mesophases. However, the three parameter Haller's extrapolation method [95] has been considered in this investigation by which the value of Δn_o (birefringence value in the crystalline state) can be estimated.

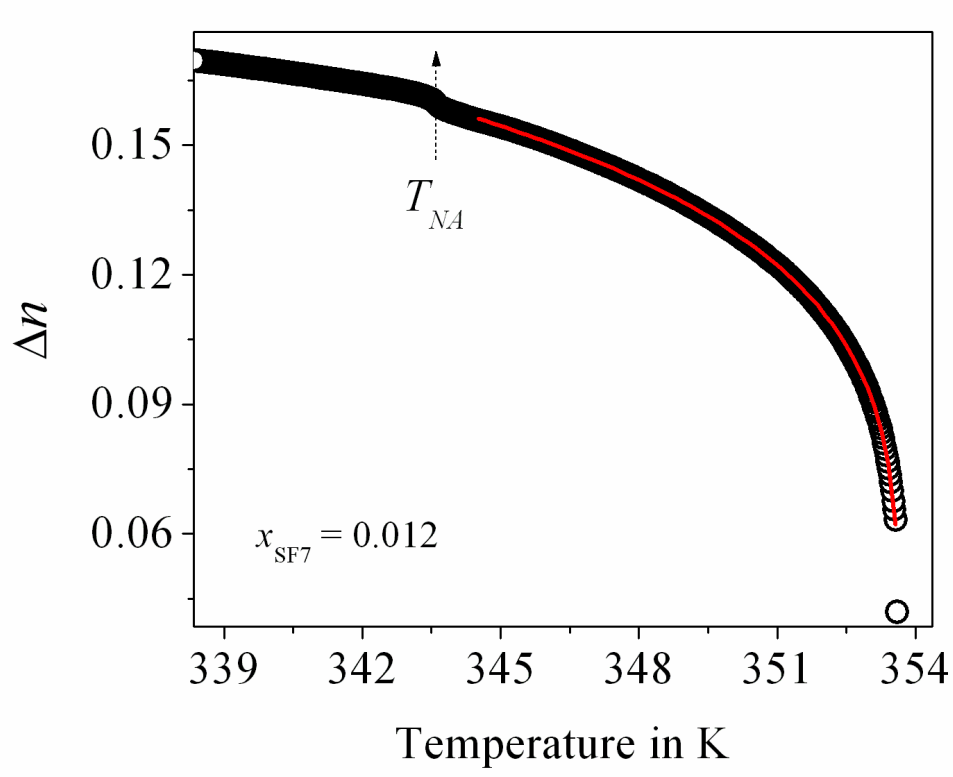

Figure 4.13. Temperature dependence of optical birefringence data for x_{SF7} = 0.012. Dashed arrow denotes the Nematic–Smectic-*A* transition temperature (T_{NA}). The solid line is a fit to Eq. (4.9).

This method is convenient in this case because of the unavailablity of density values and this procedure does not consider any local field to the LC molecule. Hence, the temperature dependence of optical birefringence data has been fitted with the expression:

$$\Delta n = \Delta n_0 \left(1 - \frac{T}{T_{IN}}\right)^{\beta} \tag{4.9}$$

where Δn_0 is the extrapolated birefringence in the perfectly ordered state (T= 0 K) and β is the critical exponent which depends on the molecular structure. The value of the orientational order parameter $\langle P_2 \rangle$ determined by the relation [88]:

$$\langle P_2 \rangle = \frac{\Delta n}{\Delta n_0} \tag{4.10}$$

The best fitted curve to Eq. (4.9) in the nematic phase has been represented in Fig. 4.13 for the investigated mixture x_{SF7} = 0.012, while the corresponding best fitted parameters Δn_0 and β for all the mixtures are listed in Table 4.4.

Table 4.4. Values of the fitting parameters Δn_0 and β obtained from Haller's fit.

x_{SF7}	Δn_0	β
0	0.319±0.001	0.195±0.001
0.012	0.323±0.001	0.198±0.001
0.03	0.336±0.003	0.214±0.003
0.05	0.344±0.013	0.215±0.006
0.065	0.365±0.011	0.220±0.006

The extracted critical exponent β is found to lie within a range from 0.195 to 0.220 for different mixtures. A discrepancy of critical exponent β value has also been arises with the theoretical values due to the incompatibility of Haller's technique with the weakly first-order character of the isotropic-nematic (*I*-*N*) phase transition [96-100].

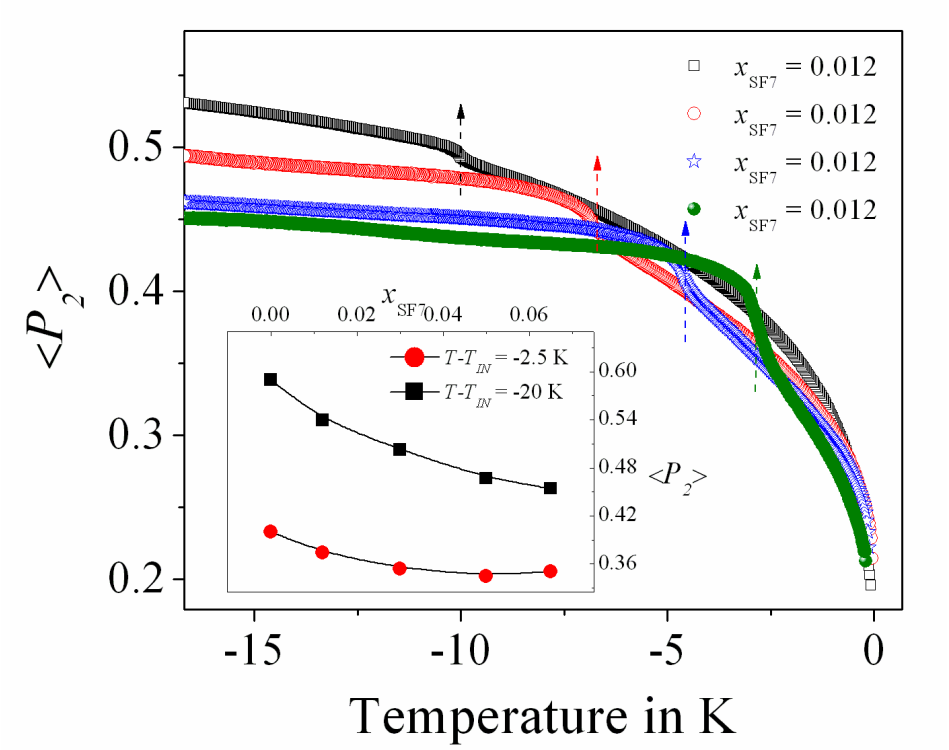

Figure 4.14. The temperature dependence of orientational order parameter (<P_2>) for all the mixtures. Dashed arrow denotes the nematic–smectic-*A* (T_{NA}) transition temperatures respectively. Inset represents the value of <P_2> at a particular temperature in both nematic and smectic phases for all the mixtures.

The temperature variation of the orientational order parameter (<P_2>) for all the investigated mixtures is represented in Fig. 4.14. It has been observed that in the vicinity of isotropic–nematic phase transition the order parameter value sharply increases, exhibiting a first order nature of *I*–*N* phase transition. Further decreasing the temperature, <P_2> value reveals a regular increase in the nematic phase due to development of the molecular orientational ordering within the medium. In the vicinity of nematic–smectic-*A* phase transition a continuous change has been identified in the order parameter data for all the mixtures under study. This continuous variation signaling a second order nature of the *N*–Sm-*A* phase transition. However, by increasing the amount of hockey stick-shaped compound, the orientational order parameter value slightly decreases which is shown in inset of Fig. 4.14 both in the nematic and smectic phases. Moreover, due to the rapid enhancement of

cluster size at very close to the *N*–Sm-*A* phase transition produces a strong pretransitional fluctuation.

Consequently, a plot of ln ($\gamma_1/\langle P_2\rangle$) with the variation of ($1/T$) gives a straight line having a slope of (E_a/k_β), from which E_a can easily be obtained. Fig. 4.15 illustrates a systematic variation of ln($\gamma_1/\langle P_2\rangle$) with ($1/T$) for all the mixtures. Therefore, the activation energy E_a has been calculated from the slope of this Arrhenius plot and listed in Table 4.5.

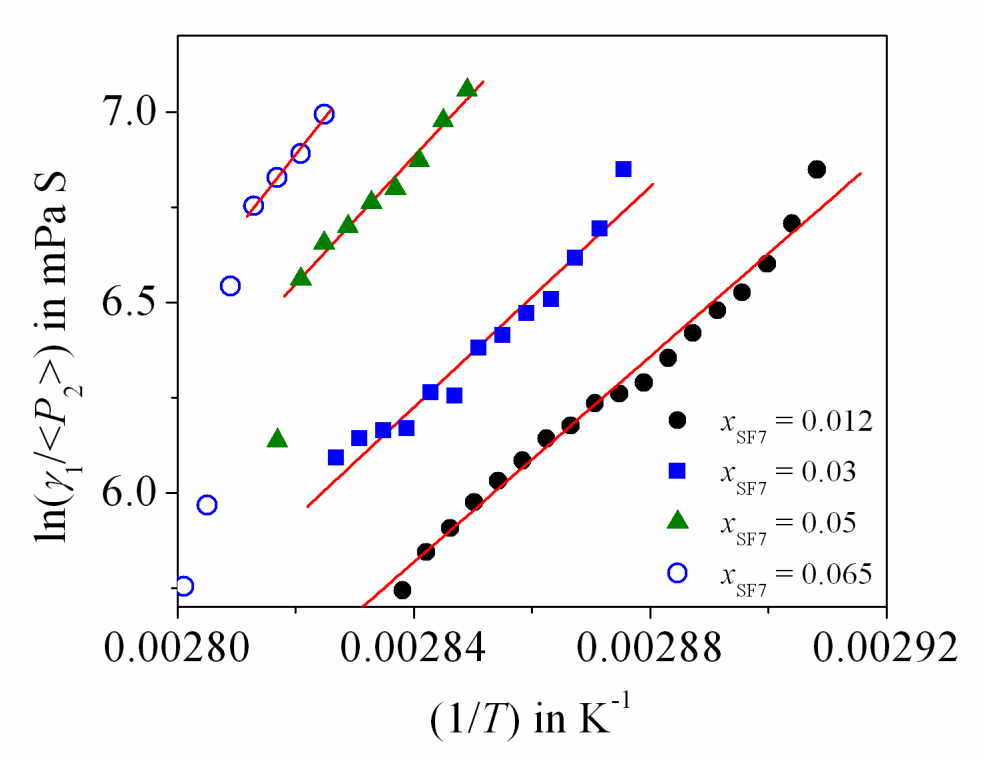

Figure 4.15. The variations of ln($\gamma_1/\langle P_2\rangle$) with reciprocal of temperature ($1/T$) for all the concentrations only in nematic phase. Solid lines represent a linear fit to the data points.

Table 4.5. Activation energies for all the mixtures in the nematic phase.

x_{SF7}	Slope (E_a/k_β)	E_a (kJmol^{-1})
0.012	13505.26	112.29
0.03	14482.32	120.41
0.05	16729.87	139.10
0.065	19687.59	163.69

Table 4.5 reveals that the activation energy for the mixture having lowest concentration (x_{SF7} = 0.012) is 112.29 kJ/mol which is quite large in comparison to that of usual calamitic compounds. Further increasing the hockey stick-shaped host compound, the activation energy monotonically increases up to a maximum value 163.69 kJ/mol for the highest concentration x_{SF7} = 0.065. These obtained results demonstrate that due to addition of SF7 compound, the intermolecular packing increases as well as a strong anti-parallel polar correlation is being developed within the rod-like environment which affects the molecular motion and thereby increases the activation energy.

4.7. Conclusion

The static dielectric and visco-elastic properties of some binary mixtures consisting of a hockey-stick shaped mesogen (SF7) with a calamitic mesogen (8OCB) have been carried out. Two different structural conformations play a significant role in the mixture leading to a noticeable shrinkage in the nematic width and impart an influence on the physical properties of the mixtures. All of the investigated mixtures possess a large positive dielectric anisotropy ($\Delta\varepsilon$), although the value of $\varepsilon_{\parallel}$ and $\Delta\varepsilon$ demonstrates a noticeable decrease by increasing the dopant concentration due to the strong polar interaction of anti-parallel aligned dipoles for both the diverse shaped mesogens. The extracted critical exponent value α'' obtained from the analysis of pretransitional behavior in ε_{iso} as well as ε_{avg} data in the vicinity of *I*–*N* phase transition assumes a value nearly equal to 0.5 within a valid error limit which clearly implies a tricritical character of the *I*-*N* phase transition for all the investigated mixtures. Moreover, by suitably employing the temperature-dependent dielectric anisotropy ($\Delta\varepsilon$) data in the vicinity of *N*–Sm-*A* phase transition, the order character of this transition has been determined by a quite similar procedure used to obtain the same in high-resolution optical birefringence data. Based on the obtained results, the *N*–Sm-*A* phase transition for all the mixtures signifying a second-order type of transitional nature and the extracted non-

universal values of the critical exponents divulges a systematic concentration variation. The critical exponents are found to reveal an excellent consistency obtained from the high-resolution optical birefringence measurements for the same binary system. Furthermore, the visco-elastic properties such as the splay elastic constant (K_{11}) and the rotational viscosity (γ_1) has been determined throughout the nematic phase for all the mixtures which also exhibit a systematic temperature and concentration dependency. By decreasing the temperature, both are found to increase gradually due to increases in molecular orientational ordering in the nematic phase. However, the efficient packing of these diverse molecules develops some temporary polar clusters within the rod-like environment having smectic-like strong short-range ordering. On increasing the amount of hockey stick-shaped mesogen, greater number of clusters developed within the system which is reflected by an increasing trend for the relative magnitude of both K_{11} and γ_1. Additionally, a pretransitional effect in the vicinity of *N*–Sm-*A* phase transition has also been observed in the experimental K_{11} and γ_1 data due to rapid enhancement in size of the clusters by decreasing the temperature. The obtained values of γ_1 for all of the investigated mixtures (consisting of hockey stick-shaped mesogen) have been found in between that of the usual calamitic compounds and that of the typical bent-core compounds. The activation energy (E_a) reveals a smaller value for the lowest concentration and further increases with increasing the dopant concentration signifying an enhancement in intermolecular packing for the addition of dopant molecule which affects the molecular motion within the system. The entire observations made in the present system shows that due to the introduction of hockey stick-shaped mesogen effectively deteriorating the nematic phase range within the mixtures and depending upon the nematic range the *N*–Sm-*A* phase transition exhibit a crossover character from second order to first order in nature.

References:

[1] P.F. McManamon, P.J. Boos, M.J. Escuti, J. Heikenfeld, S. Serati, H. Xie, and E.A. Watson, *Proc. IEEE,* **97**, 1078 (2009).

[2] A. Liu, L. Liao, D. Rubin, H. Nguyen, B. Ciftcioglu, Y. Chetrit, N. Izhaky, and M. Paniccia, *Opt. Express*, **2**, 660 (2007).

[3] V.A. Ezhov, in *Autostereoscopic display with full-screen 3D resolution (versions) and a method of controlling an active parallax barrier of the display*, Russian Federation Patent No. RU 2490818 (2012).

[4] S.A. Studentsov, and V.A. Ezhov, in *Multistandard liquid-crystal stereo glasses*, Russian Federation Patent No. RU 2488150 (2011).

[5] V.A. Ezhov, A.G. Sobolev, I.N. Kompanets, and A.L. Andreev, *Active liquid-crystal stereo glasses*, Russian Federation Patent No. RU 2456649 (2010).

[6] J. Harden, B. Mbanga, N. Eber, K. Fodor-Csorba, S. Sprunt, J.T. Gleeson, and A. Jakli, *Phys. Rev. Lett.*, **97**, 157802 (2006).

[7] A. Jakli, M. Chambers, J. Harden, M. Madhabi, R. Teeling, J. Kim, Q. Li, G.G. Nair, N. Eber, K. Fodor-Csorba, J.T. Gleeson, and S. Sprunt, *Proc. SPIE*, **6911**, 691105 (2008).

[8] S.T. Wu, *Opt. Eng.*, **26**, 120 (1987).

[9] B. Bahadur, in *Liquid crystals: applications and uses*, World Scientific, Singapore (1991).

[10] B.R. Ratna, and R. Shashidhar, *Mol. Cryst. Liy. Cryst.*, **42**, 113 (1977).

[11] M. Schadt, *The Journal of Chemical Physics*, **56**, 1494 (1972).

[12] J. Li, M. Hu, J. Li, Z. An, X. Yang, Z. Yang, and Z. Che, *Liq. Cryst.*, **41**, 1783 (2014).

[13] G.R. Luckhurst, *Thin Solid Films*, **393**, 40 (2001).

[14] R. Berardi, L. Muccioli, and C. Zannoni, *J. Chem. Phys.*, **128**, 024905 (2008).

[15] R. Balachandran, V. P. Panov, J. K. Vij, A. Lehmann, and C. Tschierske, *Phys. Rev. E*, **88**, 032503 (2013).

[16] N. Avci, V. Borshch, D.D. Sarkar, R. Dev. G. Venkatesh, T. Turiv, S. J. Shiyanovskii, N.V.S. Rao, and O.D. Lavrentovich, *Soft Matter*, **9**, 1066 (2013).

[17] B.R. Acharya, A. Primak, T.J. Dingermans, E.T. Samulski, and S. Kumar, *Pramana*, **61**, 231 (2003).

[18] B.R. Acharya, A. Primak, and S. Kumar, *Phys. Rev. Lett.*, **92**, 145506 (2004).

[19] L.A. Madsen, T.J. Dingemans, M. Nakata, and E.T. Samulski, *Phys. Rev. Lett.*, **92**, 145505 (2004).

[20] R. Stannarius, A. Eremin, M.-G. Tamba, G. Pelzl, and W. Weissflog, *Phys. Rev. E*, **76**, 061704 (2007).

[21] B. Das, S. Grande, W. Weissflog, A. Eremin, M.W. Schröder, G. Pelzl, S. Diele, and H. Kresse, *Liq.Cryst*., **30**, 529 (2003).

[22] R. Stannarius, L. Jianjun, and W. Weissflog, *Phys. Rev. Lett.*, **90**, 025502 (2003).

[23] J. Harden, R. Teeling, J.T. Gleeson, S. Sprunt, and A. Jakli, *Phys. Rev. E*, **78**, 031702 (2008).

[24] A. Chakraborty, M.K. Das, B. Das, A. Lehmann, and C. Tschierske, *Soft Matter*, **9**, 4273 (2013).

[25] A. Chakraborty, M.K. Das, B. Das, U. Baumeister, and W. Weissflog, *J. Mater. Chem. C*, **1**, 7418 (2013).

[26] B. Kundu, R. Pratibha, and N.V. Madhusudana, *Phys. Rev. Lett.*, **99**, 247802 (2007).

[27] P. Sathyanarayana, M. Mathew, Q. Li, V.S.S. Sastry, B. Kundu, K.V. Le, H. Takezoe, and S. Dhara, *Phys. Rev. E*, **81**, 010702 (2010).

[28] M. Majumdar, P. Salamon, A. Jákli, J.T. Gleeson, and S. Sprunt, *Phys. Rev. E*, **83**, 031701 (2011).

[29] P. Satyanarayana, S. Radhika, B.K. Sadashiva, and S. Dhara, *Soft Matter*, **8**, 2322 (2012).

[30] E. Dorjgotov, K. Fodor-Csorba, J.T. Gleeson, S. Sprunt, and A. Jakli, *Liq. Cryst.*, **35**, 149 (2008).

[31] P. Sathyanarayana, T. Arun Kumar, V.S.S. Sastry, M. Mathews, Q. Li, H. Takezoe, and S. Dhara, *Appl. Phys. Express*, **3**, 091702 (2010).

[32] H. Takezoe, and Y. Takanishi, *Jpn. J. Appl. Phys.*, **45**(2A), 597 (2006).

[33] O. Francescangeli, and E.T. Samulski, *Soft Matter*, **6**, 2413 (2010).

[34] T. Niori, T. Sekine, J. Watanabe, T. Furukawa, and H. Takezoe, *J. Mater. Chem*., **6**, 1231 (1996).

[35] S. Chakraborty, A. Chakraborty, and M.K. Das, *J. Mol. Liq.*, **219**, 608 (2016).

[36] V. Fréedericksz, and V. Zolina, *Trans. Faraday Soc*., **29**, 919 (1933).

[37] H.L. Ong, *Phys. Rev. A*, **33**, 3550 (1986).

[38] H. Gruler, T.J. Schiffer, and G. Meier, *Z. Natureforsh*., **27A**, 966 (1972).

[39] H. Gruler, and L. Cheung, *J. Appl. Phys.*, **46**, 5097 (1975).

[40] M.J. Bradshaw, and E.P. Rayens, *Mol. Cryst. Liq. Cryst.*, **72**, 35 (1981).

[41] Hp. Schad, *J. Appl. Phys.*, **54**, 4994 (1983).

[42] J. Jadzyn, and G. Czechowski, *Liq. Cryst.*, **4**, 157 (1989).

[43] S. Sridevi, S.K. Prasad, D.S. Shankar Rao, C.V. Yelamaggad, *J. Phys.: Condens. Matter*, **20**, 465106 (2008).

[44] S.K. Sarkar, and M.K. Das, *Fluid Phase Equilib*., **365**, 41 (2014).

[45] A. Drozd-Rzoska, S.J. Rzoska, and J. Zioło, *Phys. Rev. E*, **55**, 2888 (1997).

[46] M. Janik, S.J. Rzoska, A. Drozd-Rzoska, and J. Zioło, *The Journal of Chemical Physics*, **124**, 144907 (2006).

[47] S.J. Rzoska, J. Ziolo, W. Sulkoski, J. Jadżyn, and G. Czechowski, *Phys. Rev. E*, **64**, 052701 (2001).

[48] M. Ginovska, H. Kresse, D. Bauman, G. Czechowski, and J. Jadzyn, *Phys. Rev. E*, **69**, 022701 (2004).

[49] J. Jadżyn, G. Czechowski, and J.-L. Déjardin, *J. Phys.: Condens. Matter*, **18**, 1839 (2006).

[50] D. Wiant, S. Stojadinovic, K. Neupane, S. Sharma, K. Fodor-Csorba, A. Jákli, J. T. Gleeson, and S. Sprunt, *Phys. Rev. E*, **73**, 030703 (2006).

[51] P.K. Mukherjee, and T.B. Mukherjee, *Phys. Rev. B*, **52**, 9964 (1995).

[52] P.K. Mukherjee, *J. Phys. Condens. Matter*, **10**, 9191 (1998).

[53] A. Drozd-Rzoska, *Phys. Rev. E*, **59**, 5556 (1999).

[54] A. Drozd-Rzoska, S.J. Rzoska, J. Ziolo, *Phys. Rev. E*, **54**, 6452 (1996).

[55] P. Cusmin, M.R. de la Fuente, J. Salud, M.A. Pérez-Jubindo, S. Diez-Berart, and D.O. López, *J. Phys. Chem. B*, **111**, 8974 (2007).

[56] J. Jadzyn, G. Czechowski, and J.L. Déjardin, *J. Phys. Condens. Matter*, **18**, 1839 (2006).

[57] A. Drozd-Rzoska, and S.J. Rzoska, in *Phase Transition: Application to liquid crystal, Organic Electronics and Optoelectronics Fields*, (Fifth Ed.) Popa-Nita, Trivandrum: Research Signpost (2006).

[58] S. Parthasarathi, D.S. Shankar Rao, K.F. Csorba, and S.K. Prasad, *J. Phys. Chem. B*, **118**, 14526 (2014).

[59] S. Parthasarathi, D.S. Shankar Rao, N.B. Palakurthi, C.V. Yelamagad, and S.K. Prasad, *J. Phys. Chem. B*, **120**, 5056 (2016).

[60] P.H. Keyes, *Phys. Lett. A*, **67**, 132 (1978).

[61] M.A. Anisimov, S.R. Garber, V.S. Episov, V.M. Mamnitskii, G.I. Ovodov, L.A. Smolenko, and E.L. Sorkin, *Sov. Phys. JETP*, **45**, 1042 (1977).

[62] M.A. Anisimov, *Mol. Cryst. Liq. Cryst. Inc. Nonlinear Opt.*, **162**, 1 (1988).

[63] S. Yildiz, H. Özbek, C. Glorieux, and J. Thoen, *Liq. Cryst.*, **34,** 611 (2007).

[64] S. Erkan, M. Çetinkaya, S. Yildiz, and H. Özbek, *Phys. Rev. E*, **86**, 041705 (2012).

[65] A. Chakraborty, S. Chakraborty, and M.K. Das, *Phys. Rev. E*, **91**, 032503 (2015).

[66] L.M. Blinov, and V.G. Chigrinov, in *Electro-optic effects in liquid crystal materials*, Springer-Verlag, New York (1994).

[67] S. DasGupta, P. Chattopadhyay, and S.K. Roy, *Phys. Rev. E.*, **63**, 041703 (2001).

[68] S. DasGupta, and S.K. Roy, *Liq. Cryst.*, **30**, 31 (2003).

[69] S. DasGupta, and S.K. Roy, *Phys. Lett. A*, **306**, 235 (2003).

[70] S.W. Morris, P. Palffy-muhoray, and D.A. Balzarini, *Mol. Cryst. Liq. Cryst.*, **139**, 263 (1986).

[71] D.V. Sai, K.P. Zuhail, R. Sarkar, and S. Dhara, *Liq. Cryst.*, **42**, 328 (2015).

[72] P. Tadapatri, U.S. Hirenath, C.V. Yelamaggad, and K.S. Krishnamurthy, *J. Phys. Chem. B*, **114**, 1745 (2010).

[73] P. Satyanarayana, M. Mathew, Q. Li, V.S.S. Sastry, B. Kundu, K.V. Le, H. Takezoe, and S. Dhara, *Phys. Rev. E*, **81**, 010702 (2010).

[74] S. Kaur, J. Addis, C. Greco, A. Ferrarini, V. Görtz, J.W. Goodby, and H.F. Gleeson, *Phys. Rev. E*, **86**, 041703 (2012).

[75] G. Czechowski, and J. Jadzyn, *Acta Physica Polonica A*, **106**, 475 (2004).

[76] A. Chakraborty, S. Chakraborty, M.K. Das, and W. Weissflog, *J. Mol. Liq.*, **265**, 536 (2018).

[77] P. Satyanarayana, B.K. Sadashiva, and S. Dhara, *Soft matter*, **7**, 8556 (2011).

[78] S.T. Wu, and C.S. Wu, *Phys. Rev. A*, **42**, 2219 (1990).

[79] M.L. Dark, M.H. Moore, D.K. Shenoy, and R. Shashidhar, *Liq. Cryst.*, **33**, 67 (2006).

[80] A.V. Zakharov, and R.Y. Dong, *Eur. Phys. J. E*, **7**, 267 (2002).

[81] P.G. de Gennes, *Solid State Commun.*, **10**, 753 (1972).

[82] F. Jähnig, and F. Brochard, *J. Phys.*, **35**, 301 (1974).

[83] D.R. Kim, *J. Korean Phys. Soc.*, **32**, 55 (1998).

[84] W.L. McMillan, *Phys. Rev. A*, **9**, 1720 (1974).

[85] H. Kneppe, F. Schneider, and N.K. Sharma, *J. Chem. Phys.*, **77**, 3203 (1982).

[86] A. Pramanik, B. Das, M.K. Das, K. Garbat, S. Urban, and R. Dabrowski, *Liq. Cryst.*, **40**, 149 (2013).

[87] G.W. Gray, V. Vill, H.W. Spiess, D. Demus, and J.W. Goodby, in *Physical properties of liquid crystals*, Wiley-VCH, Singapore (1999).

[88] W.H. de Jeu, in *Physical properties of liquid crystalline materials*, Gordon and Breach, New York (1980).

[89] P.G. de Gennes, in *The physics of liquid crystals*, Clarendon Press, Oxford (1974).

[90] W. Kuczynski, B. Zywucki, and J. Malecki, *Mol. Cryst. Liq. Cryst.*, **381**, 1 (2002).

[91] P. Pardhasaradhi , P.V.D. Prasad , D.M. Latha , V.G.K.M. Pisipati, and G.P. Rani, *Phase Transit.*, **85**, 1031 (2012).

[92] K.D. Thingujama, P.R. Alapati, B. Choudhury and A. Bhattacharjee, *Phase Transit.*, **85**, 52 (2012).

[93] A. Kumar, *Liq. Cryst.*, **40**, 203 (2013).

[94] M. K. Das, G. Sarkar, B. Das, R. Rai, and N. Sinha, *J. Phys.: Condens. Matter*, **24**, 115101 (2012).

[95] I. Haller, *Prog. Solid State Chem*., **10**, 103 (1975).

[96] A. Prasad, and M.K. Das, *Phase Transit*., **83**, 1072 (2010).

[97] M. Mitra, and R. Paul, *Mol. Cryst. Liq. Cryst.*, **148**, 185 (1987).

[98] P.D. Roy, B. Das, and M.K. Das, *J. Phys.: Condens. Matter*, **21**, 335108 (2009).

[99] P.D. Roy, A. Prasad, and M.K. Das, *J. Phys.: Condens. Matter*, **21**, 075106 (2009).

[100] S.D. Sarkar, B. Choudhury, and M.K. Das, *Phase Transit.*, **85**, 85 (2012).